Songklanakarin J. Sci. Technol.
40 (3), 659-665, May - Jun. 2018

http://www.sjst.psu.ac.th

Original Article

Photocatalytic antibacterial performance of PVP-doped SnO_2/TiO_2 thin films coated on glass fibers

Peerawas Kongsong[1*], Lek Sikong[2], Mahamasuhaimi Masae[3], Witawat Singsang[1], Sutham Niyomwas[4], and Vishnu Rachpech[2]

[1]*Department of Materials Engineering, Faculty of Engineering and Architecture, Rajamangala University of Technology Isan, Mueang, Nakhon Ratchasima, 30000 Thailand*

[2]*Department of Mining and Materials Engineering, Faculty of Engineering, Prince of Songkla University, Hat Yai, Songkhla, 90112 Thailand*

[3]*Department of Industrial Engineering, Faculty of Engineering, Rajamangala University of Technology Srivijaya, Mueang, Songkhla, 90000 Thailand*

[4]*Department of Mechanical Engineering, Faculty of Engineering, Prince of Songkla University, Hat Yai, Songkhla, 90112 Thailand*

Received: 23 December 2016; Revised: 7 February 2017; Accepted: 21 March 2017

Abstract

PVP (polyvinylpyrrolidone)-doped SnO_2/TiO_2 composite thin films and undoped films were prepared by sol-gel and dip-coating methods. The calcined films at 600 ^oC for 2 h were characterized by scanning electron microscopy, X-ray defractometer, UV-Vis spectroscopy, and X-ray photoelectron spectroscopy. Furthermore, the photocatalytic reaction on the degradation of methylene blue dye solution was also investigated in order to observe the correlation between the results of bacteria inactivation of the prepared films and that of photocatalytic activity on methylene blue degradation. The PVP-doped SnO_2/TiO_2 composite thin films and undoped films were preliminarily studied against gram negative *Escherichia coli* and gram positive *Staphylococcus aureus* bacteria. It revealed that PVP-doped SnO_2/TiO_2 composite films resulted in shifting the absorption wavelength towards narrowing the energy band gap, high crystallinity of anatase phase, and small crystallite size. Therefore, the 40PVP/SnO_2/TiO_2 composite thin film exhibited greater photocatalytic activity and water disinfection efficiency than those of undoped films.

Keywords: PVP doped SnO_2/TiO_2, glass fiber, water disinfection, *Escherichia coli*, *Staphylococcus aureus*

1. Introduction

Groundwater contamination by pathogenic organisms is an important concern due to overgrowing populations with limited access to sanitation and safe drinking water. Urban population growth and higher demands on agricultural yield to feed an increasing number of people would eventually lead to detrimental effects on groundwater quality (Gentile *et al.*, 2016). Contaminated water commonly contains dangerous pathogens, and its consumption creates serious health effects and societal problems. In the past decade, many innovative disinfection technologies were developed and adopted as alternatives to chlorine and ozone associated disinfection processes, including germicide ultraviolet (UV) radiation and photocatalytic oxidation. The traditional disinfection approaches have potential risks, such as carcinogenic by–

*Corresponding author
Email address: physics_psu@windowslive.com

products (DBPs). For the alternative technologies, diverse nano photocatalysts such as titanium dioxide (TiO_2), zinc oxide (ZnO), cadmium sulfide (CdS), and silver nanoparticles, have been widely studied and are considered promising, due to their unique properties including large specific area and high reactivity (Gao *et al.,* 2012)

TiO_2 is the most commonly used semiconductor photocatalyst. Among the different nanomaterials, it is the most studied. Activated by UV-A irradiation, its photocatalytic properties have been utilized in various environmental applications to remove contaminants from both water and air. A wealth of information on TiO_2 photocatalytic inactivation of bacteria has been acquired over the last 20 years. TiO_2 can kill both gram negative and gram positive bacteria, although gram positive bacteria have a protective, thick peptidoglycan layer in the cell wall. The exact bactericidal mechanism of reactive oxygen species (ROS) is not yet fully known, but the photocatalytic activity of TiO_2 produces them, and they are extremely reactive killing or deactivating microorganisms on contact (Li *et al.,* 2008).

There are many techniques to improve photoactivity such as control of phase, morphology crystallite size, and band gap energy reducing. Doping TiO_2 with N and SnO_2 could extend the photochemical activity (Qin *et al.,* 2008; Chen *et al.,* 2009), as metal and metal oxides are known to enhance the activity (Chen *et al.,* 2009; Sikong *et al.,* 2012).

Nitrogen-doped TiO_2 is attracting continuously increasing attention because of its potential as a material for environmental photocatalysis. Many authors have reported on N-doped TiO_2. Although some authors claim that the band gap of the solid is reduced due to a rigid valence band shift upon doping, others attribute the observed absorption of visible light by N–TiO_2 to the excitation of electrons from localized impurity states in the band gap. Interestingly, it appears that the N–doping-induced modifications of the electronic structure may be slightly different for the anatase and rutile polymorphs of TiO_2 (Valentin *et al.,* 2007; Vaiano *et al.,* 2017).

The aim of this work was to investigate the water disinfection efficiency of PVP–doped and undoped SnO_2/TiO_2 composite films under UV radiation. The quantity of dopants in TiO_2 films was varied. The PVP–doped and undoped SnO_2/TiO_2 composite films were formed as coatings on glass fibers, and the photocatalytic antibacterial effects of these films against gram negative *Escherichia coli* and gram positive *Staphylococcus aureus* were assessed. The fraction of viable bacteria that survived the treatment was determined with the spread plate technique. Furthermore, photocatalytic degradation of methylene blue (MB) dye in solution was also investigated, to correlate this activity with antibacterial activity.

2. Experimental

2.1 Materials and methods

Three layers of coating were deposited on glass fibers of type E–glass by the sol–gel process using the dip–coating method. The specific surface area of the starting glass fiber materials was 0.05 m^2g^{-1} and the diameter was about 20 µm. The coating of the sol-gel for the first film layer was SiO_2/TiO_2 prepared by dissolving 9 ml of titanium tetra–isopropoxide (TTIP, 99.95%, Fluka Sigma–Aldrich) and 0.07 ml of tetraethylorthosilicate (TEOS, 98%, Fluka Sigma–Aldrich) in 145 ml of ethanol and stirred at room temperature at a speed of 800 rpm for 60 min to achieve the mole ratio of TTIP : C_2H_5OH = 1:82 then adding 2 M HCl into the sol-gel to adjust the pH to about 3.5. The coating sol-gel for the second and third layers were the PVP–doped SnO_2/TiO_2 composite, prepared by dissolving certain amounts of TTIP, polyvinylprrrolidone (PVP), and 0.315 g of tin (IV) chloride pentahydrate (98%, Riedel DeHaën) in 145 ml of ethanol and stirred at room temperature at a speed of 800 rpm for 60 min. Then 2 M HCl was added to the sol-gel to adjust the pH to about 3.5. The concentration of SiO_2 in TiO_2 of the first layer was fixed at 5 mol%, while in the second and third layers 3 mol% SnO_2 was used. PVP of 0–40 mol% was doped into the SnO_2/TiO_2 composite films following Hao–Li Qin and co–workers (Qin *et al.,* 2008).

Before coating, the glass fibers were heated at 500 °C for 1 h in order to remove wax, cleaned in an ultrasonic bath using ethanol, and dried at 105 °C for 24 h. A dip–coating apparatus was used to coat the fibers. At first, SiO_2/TiO_2 sol was coated on glass fibers as a compatibilizer layer and followed with PVP–doped SnO_2/TiO_2 solution on top for another two layers. The sol-gel could be homogenously coated on the substrate at the dipping speed of 1.0 mm/s. Secondly, gel films of TiO_2 composites were obtained by drying at 60 °C for 30 min before calcination at 600 °C for 2 h at a heating rate of 10 °C/min. After that the TiO_2 composite films coated glass fibers were cleaned with distilled water in an ultrasonic bath for 15 min to remove the TiO_2 free particles, dried at 105 °C for 24 h, and kept in a desiccator until use in the experiments.

2.2 Materials characterization

The surface morphologies of the prepared films were characterized by scanning electron microscopy (SEM, Quanta, FEI). The chemical composition of the films was investigated by a X–ray photoelectron spectrometer (XPS; AXIS ULTRA^{DLD}, Kratos analytical, Manchester, UK). Spectrums were processed on "VISION II" software by Kratos analytical, Manchester, UK. The base pressure in the XPS analysis chamber was about 5 x 10^{-9} torr. The samples were excited with X–ray hybrid mode 700 x 300 µm spot area with a monochromatic Al $K_{\alpha\ 1,2}$ radiation at 1.4 keV. The X–ray anode was run at 15kV, 10 mA, and 150 W. The photoelectrons were detected with a hemispherical analyzer positioned at an angle of 45º with respect to the normal of the sample surface. Crystallinity composition was characterized using an X–ray diffractometer (XRD) (Phillips E'pert MPD, Cu–Kα). The crystallite size was determined from XRD peaks using the Scherer equation (Liuxue *et al.,* 2006),

$$D=0.9\lambda/\beta\cos\theta_\beta \quad (1)$$

where D is the crystallite size, λ is the wavelength of X–ray radiation (Cu–Kα = 0.15406 nm), β is the angle width at half of the maximum height, and θ_β is the half diffraction angle of the centroid of the peak in degrees. The band gap energies of TiO_2 and TiO_2 composites, in powder form, were measured by

a UV–Vis–NIR spectrometer with an integrating sphere attachment (Shimadzu ISR–3100 spectrophotometer), using $BaSO_4$ as reference.

2.3 Photocatalytic reaction test

The photocatalytic activity of TiO_2, PVP-doped SnO_2/TiO_2 thin films coated on glass fiber substrates was tested by means of degradation of a MB solution (50 ml) having an initial concentration of 1 x 10^{-5} M with 1 g of the undoped or doped TiO_2 glass fibers using a UV-lamp (black light) of 50 W power and an irradiated intensity of 310-400 nm wavelength. The distance between the testing substrate and a light source was 32 cm. The photocatalytic reaction test was done in a dark chamber under UV irradiation at various times up to 4 h. The remaining concentration of MB was determined by UV-Vis spectrophotometer.

2.4 Photocatalytic antibacterial measurements

E. coli and *S. aureus* were obtained from the Microbiology Science Laboratory, Prince of Songkla University, Songkhla. Bacteria cells were grown aerobically in 4 ml of tryticase soy broth at 37 °C for 24 h. Then the bacterial solution was diluted in saline solution (0.85% NaCl) until the number of bacteria was in the range of 30–300/ml. The number of viable bacteria in a treated solution can be readily quantified using spread plate technique in which a sample is appropriately diluted and transferred to an agar plate. After colonies are grown, they are counted and the number of bacteria in the original sample is calculated. It was found that the initial bacterial concentration is an important factor in evaluating the antibacterial efficiency (Zhang *et al.*, 2008). The initial bacterial concentration was kept about 10^3 CFU/ml. An aliquot of 50 ml of bacteria suspension was mixed with TiO_2 composite films coated on the glass fibers 40 g/l. The mixture was then exposed to irradiation of UV at different time. Then, 1 ml of mixture suspension was sampled, added to the MacConkey agar plates for the *E. coli* and nutrient agar plates for the *S. aureus* and incubated at 37 °C for 24 h. The number of viable bacteria was determined using the spread plate technique after the photocatalytic reaction time. After incubation, the number of viable colonies of bacteria on each agar plate was observed.

3. Results and Discussion

3.1 XRD results of TiO2 thin films

Figure 1 shows the XRD patterns of the thin films which indicated that undoped and PVP-doped SnO_2/TiO_2 thin films obtained by calcination at 600 °C for 2 h were anatase crystal phase due to the presence of attributive peaks (2θ = 25.4◦, 37.6◦, 47.6◦, and 54.6◦). It means that phase transformation from amorphous to anatase structure was achieved which commonly requires a high temperature. A very broad diffraction peak at (1 0 1) plane (2θ = 25.4◦) was due to the small crystalline size of TiO_2. The crystallite sizes calculated from Scherrer's equation of TiO_2, SnO_2/TiO_2, SnO_2/TiO_2 and PVP doped SnO_2/TiO_2 are shown in Table 1. At 30 mol% PVP doped SnO_2/TiO_2 composite film calcined at 600 °C had the smallest crystallite size of 8.4 nm. PVP seems to hinder phase transformation from amorphous to anatase phase, thus PVP doped SnO_2/TiO_2 film showed a lower degree of crystallinity than the others while SnO_2/TiO_2 showed the highest degree of crystallinity (Figure 1). The samples containing more PVP may result with a thinner TiO_2 layer as a result of calcination and removal of PVP. As known, both crystallite size and degree of crystallinity have an effect on the photocatalytic reaction.

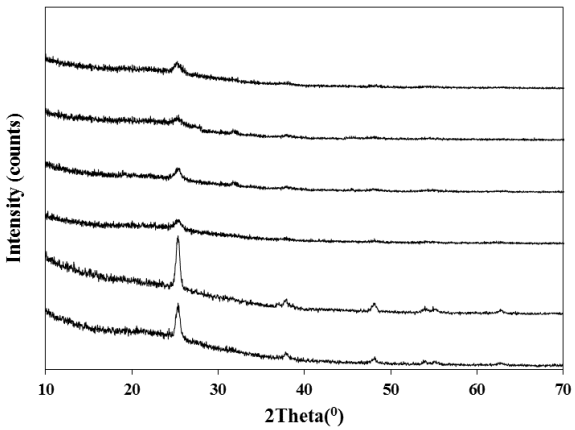

Figure 1. XRD patterns of thin films calcined at 600 °C: (a) TiO_2 (b) SnO_2/TiO_2 (c–f) 10, 20, 30 and 40 mol% PVP/SnO_2/TiO_2, respectively.

3.2 Morphology of the thin film surface

The morphologies of the TiO_2 films coated on glass fibers were observed by SEM (Figure 2). Nucleation of anatase crystallites was observed and the surface was homogeneous and smooth. However, excess TiO_2 seems to be randomly deposited on the glass fiber surfaces. Agglomeration of nanoparticles was clearly found for the SnO_2/TiO_2 film (Figure 2f) but not for the undoped TiO_2 (Figure 2d) or 40PVP/SnO_2/TiO_2 films (Figure 2h). PVP doping hindered the anatase crystal growth and reduced the crystallite size in agreement with the XRD results (Figure 1).

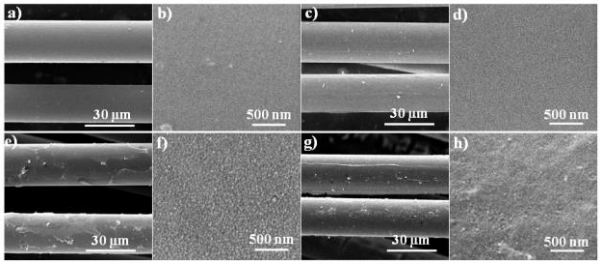

Figure 2. SEM images of glass fibers, some coated and calcined at 600 °C. (a) uncoated 1,500x, (b) uncoated 60,000x, (c) TiO_2 1,500x, (d) TiO_2 60,000x, (e) SnO_2/TiO_2 1,500x, (f) SnO_2/TiO_2 60,000x, (g) 40PVP/SnO_2/TiO_2 1,500x, and (h) 40PVP/SnO_2/TiO_2 60,000x.

3.3 Band gap energy determination

The UV–vis spectra of pure TiO_2 and composite TiO_2 are shown in Figure 3. The absorption edge of the samples was determined by the following equation:

$$E_g = 1239.8/\lambda \quad (2)$$

where E_g is the band gap energy (eV) of the sample and λ (nm) is the wavelength of the onset of the spectrum. The undoped TiO_2 catalyst exhibited absorption only in the UV region with the absorption edge around 400 nm. The band gap energies of the PVP–doped SnO_2/TiO_2 catalysts were slightly narrower than the undoped TiO_2 (3.20 eV) (Table 1). Dopants affect the UV–vis spectra by inhibiting recombination of electron–hole pairs, especially for the PVP–doped specimens. The band gap energy of PVP/SnO_2/TiO_2 shifted by 0.14–0.26 eV relative to 3.20 eV for pure TiO_2. The band gap energy of 40PVP/SnO_2/TiO_2 was 2.94 eV. The band gap energy of TiO_2 tends to decrease with increased PVP content. These shifts demonstrate how photocatalytic activity may be modulated by atomic–level doping of a nano–catalyst. The absorption wavelength of the 40PVP/SnO_2/TiO_2 photocatalyst extended towards visible light (λ = 421.7 nm), relative to the other samples (Sikong *et al.*, 2012), giving it the highest photocatalytic activity. The PVP doping slightly decreased the band gap to 2.94 eV by formation of localized N 2p states just above the valence band maximum of TiO_2 due to substitutional N species (Jaiswal *et al.*, 2012). As the amount of PVP doping increased, the degree of crystallinity of anatase (TiO_2) decreased, resulting in reduction of crystallite size. In addition, the N interstitial atoms incorporated into the TiO_2 lattice has an effect on the light absorption edge shifting to longer wave lengths in the visible region leading to the reduction of band gap energy.

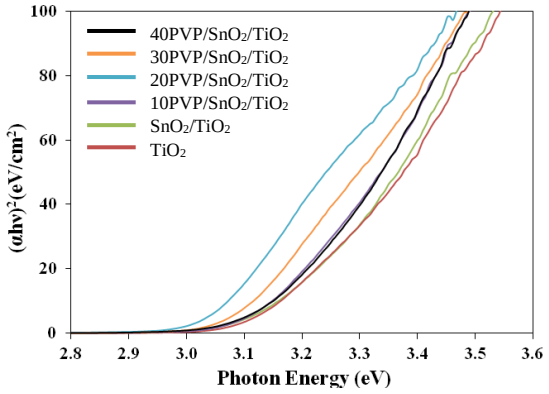

Figure 3. The photon energy versus $(\alpha h\nu)^2$ curve of representative pure TiO_2 and PVP doped SnO_2/TiO_2 samples calcined at 600 °C.

3.4 XPS analysis

Figure 4 shows the X–ray photoelectron spectroscopic (XPS) survey spectra of TiO_2 and 40PVP/SnO_2/TiO_2 thin films. The elements Ti, O, N, and Sn were clearly detected and the semi–quantitative analysis estimated the atomic fractions at 16.8, 63.7, 0.5, and 0.7%, respectively, for the 40PVP/SnO_2/TiO_2 thin film. The XPS peaks indicated that the co–doped TiO_2 thin films contained Ti, Sn, O, and N elements, and the binding energies of Ti 2p, Sn 3d, O 1s, and N 1s were 458, 496, 525, and 400 eV, respectively. The Sn 3d XPS peaks of Sn–TiO_{2-x} demonstrate existence of stannous species on the surface of the TiO_2 (Figure 5a). The Sn $3d_{5/2}$–binding energy of Sn–TiO_{2-x} at 486.1 eV was below the 486.6 eV reference value found in the literature (Xin *et al.*, 2009). To assess the state of nitrogen atoms in the 40PVP/SnO_2/TiO_2 thin films, high–resolution XPS spectra of N 1s region were generated (Figure 5b). The peak at 400.1 eV could be attributed to the interstitial nitrogen atoms in the crystal lattice of TiO_2 as a Ti–O–N structural feature (Wang *et al.*, 2015). This form of Ti-O-N linkages, reduced the band gap energy beneficially for the photocatalytic properties of 40PVP/SnO_2/TiO_2 films.

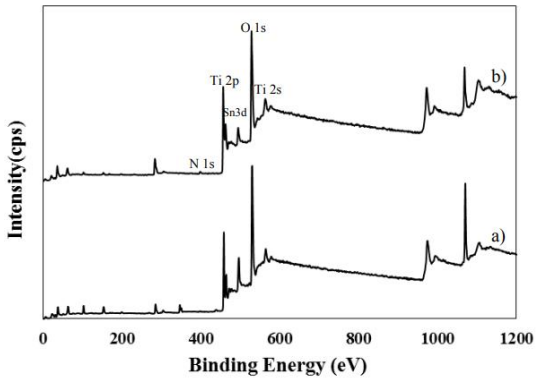

Figure 4. XPS spectra of a) TiO_2 and b) 40PVP/SnO_2/TiO_2 thin films samples calcined at 600 °C.

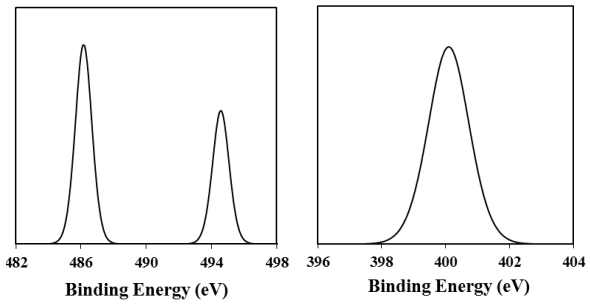

Figure 5. XPS spectrum of a) Sn 3d and b) N 1s on the surface of 40PVP/SnO_2/TiO_2 thin films samples calcined at 600 °C.

3.5 Photocatalytic activity test

The photocatalytic activity of TiO_2 and TiO_2 composite photocatalytic films was performed by means of degradation of a MB solution with an initial concentration of 1 x 10^{-5} M under UV for various irradiation times. Figure 6 is plotted between the C/C_0 ratio and UV irradiation time, where C_0 and C are the concentrations of MB at the beginning and the concentration of MB that remained after a designed treatment time, respectively. It could be seen that PVP doping has an effect on the photocatalytic activity of the as-prepared

samples and the 40PVP/SnO_2/TiO_2 thin film exhibits the optimum photoactivity (Figure 6). According to a previous report, many factors influenced the photoactivity of TiO_2 photocatalyst, such as crystalline phase, grain size, specific surface area, surface morphology, and surface state (surface OH radical) and they were closely related to each other (Zaleska *et al.*, 2008; Zhang *et al.*, 2008). Doping TiO_2 with PVP resulted in shifting light absorption wavelength to the visible region, small crystallite size, and narrowed the energy band gap (3.20 eV) (Ying *et al.*, 2008). The excellent photocatalytic activity of the well-crystallized anatase phase which facilitates the transfer of photo-induced vacancies from bulk to surface for degradation of organic composites and effectively inhibits the recombination between photo generated electrons and holes. The 30PVP/SnO_2/TiO_2 thin film exhibited the smallest crystallite size and was estimated to be about 8.4 nm (Figure 1) (Table 1).

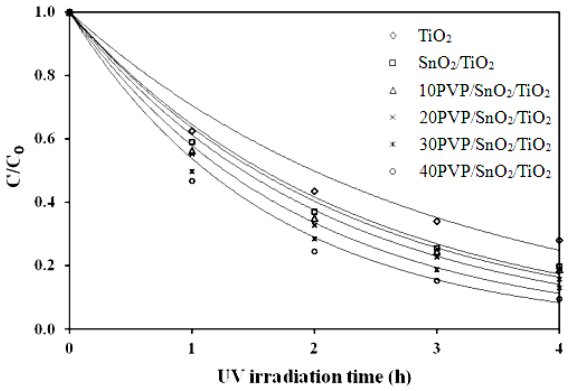

Figure 6. Photocatalytic performance on degradation of MB of TiO_2 and TiO_2 composite thin films coated on glass fiber thin films.

Table 1. Effect of PVP content on crystallite sizes, energy band gap, and photocatalytic degradation of MB for 4 h of TiO_2 and TiO_2 composite thin films synthesized at different content amounts of PVP.

Samples	crystallite size (nm)	Energy band gap (eV)	% degradation of MB for 4 h (%)
TiO_2	17.2	3.20	71.9
SnO_2/TiO_2	17.2	3.20	80.3
10PVP/SnO_2/TiO_2	12.9	3.06	81.3
20PVP/SnO_2/TiO_2	10.3	3.05	84.3
30PVP/SnO_2/TiO_2	8.4	3.01	86.9
40PVP/SnO_2/TiO_2	8.6	2.94	90.4

3.6 Photocatalytic disinfection against bacteria

The efficiency of bacteria photo-inactivation with a UV light was evaluated using distilled water containing the pathogen. The initial bacterial concentration was kept at about 10^3 CFU/ml. The survival curves of bacteria were plotted between N/N_0 ratio and time, where N_0 and N are the number of survival cells at the beginning and at a certain treatment time, respectively (Figures 7 and 8). The inactivation rate constants (k), which are direct quantitative indicators of antibacterial activity, were determined from Figures 7 and 8 for the control (uncoated glass fibers under UV irradiation) and the TiO_2, SnO_2/TiO_2, and 40PVP/SnO_2/TiO_2 films (Table 2). The k value of the 40PVP/SnO_2/TiO_2 film was higher than the other samples due to its smaller crystallite size or larger surface area.

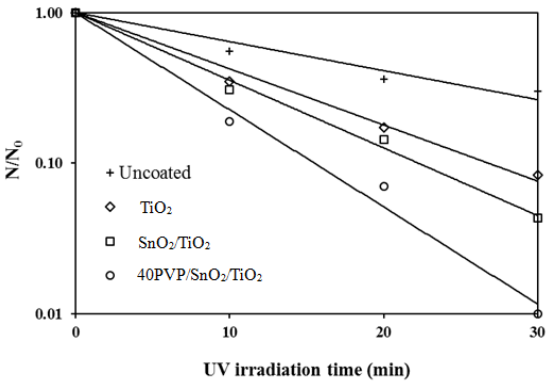

Figure 7. Antibacterial efficiency of uncoated, TiO_2 and 40PVP/SnO_2/TiO_2 composite thin films against *E. coli* under UV irradiation.

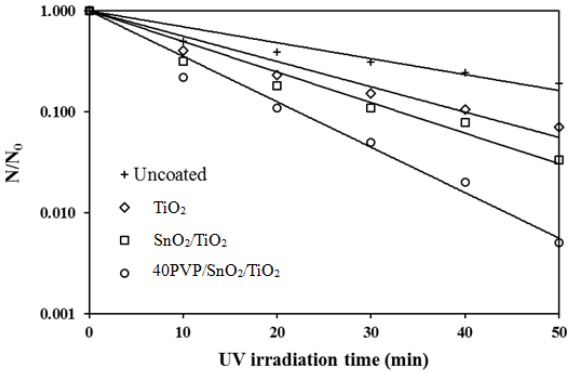

Figure 8. Antibacterial efficiency of uncoated, TiO_2 and 40PVP/SnO_2/TiO_2 composite thin films against *S. aureus* under UV irradiation.

Table 2. Summary of numerical fits of first order kinetics to the inactivation of bacteria.

Bacteria	Samples	Rate Equation	Rate constant (k)(min^{-1})	R^2
E. coli	Uncoated	$N/N_0=e^{-0.044t}$	0.044	0.935
	TiO_2	$N/N_0=e^{-0.086t}$	0.086	0.986
	SnO_2/TiO_2	$N/N_0=e^{-0.103t}$	0.103	0.993
	40PVP/SnO_2/TiO_2	$N/N_0=e^{-0.149t}$	0.149	0.987
S. aureus	Uncoated	$N/N_0=e^{-0.036t}$	0.036	0.888
	TiO_2	$N/N_0=e^{-0.058t}$	0.058	0.940
	SnO_2/TiO_2	$N/N_0=e^{-0.070t}$	0.070	0.944
	40PVP/SnO_2/TiO_2	$N/N_0=e^{-0.104t}$	0.104	0.981

The killing rate (k) was higher at 0.149 min^{-1} for *E. coli* disinfection compared to 0.104 min^{-1} for *S. aureus*. The result indicated that the 40PVP/SnO_2/TiO_2 as-prepared film exhibits higher bactericidal activity against bacteria under UV irradiation compared to uncoated pure TiO_2 and SnO_2/TiO_2 thin films. It was found that in the presence of 40PVP/SnO_2/TiO_2, *E. coli* was almost completely inactivated under UV irradiation within 30 min and completely killed within 40 min while those of the SnO_2/TiO_2, undoped TiO_2 and uncoated thin films are 98, 97 and 55%, respectively, at 40 min (Figure 7). In the presence of 40PVP/SnO_2/TiO_2, *S. aureus* was almost completely inactivated under UV irradiation within 50 min and completely killed within 60 min while those of the SnO_2/TiO_2, undoped TiO_2 and uncoated thin films were 98, 96 and 77%, respectively, at 60 min (Figure 8). The uncoated glass fiber shows significant antibacterial activity which indicated the bactericidal effect of the UV light source. It was found that the 40PVP/SnO_2/TiO_2 film had a higher antibacterial effect than undoped TiO_2. The bacterial inactivation of the prepared films correlated closely to the photocatalytic activity performed by degradation of the MB dye solution. Figure 6 illustrates the antibacterial efficiency of 40PVP/SnO_2/TiO_2 composite thin films against *E. coli* and *S. aureus* under UV irradiation. It was found that the 40PVP/SnO_2/TiO_2 film had a higher antibacterial effect on gram negative bacteria than on gram positive bacteria because gram positive bacteria have a thick cell wall composed of multilayers of peptidoglycan (Ramani *et al.*, 2012). The bactericidal effect of TiO_2 generally has been attributed to the decomposition of bacterial outer membranes by ROS, primarily hydroxyl radicals (-OH), which leads to phospholipid peroxidation and ultimately cell death. It was proposed that nanomaterials that can physically attach to a cell can be bactericidal if they come into contact with this cell (Rajakumara *et al.*, 2012). Figure 9 shows the pictures of bacteria on the agar plates observed after treatment with 40PVP/SnO_2/TiO_2 composite thin films against *E. coli* and *S. aureus* under UV irradiation. It was apparent that damage to the bacteria cell walls can take place immediately after irradiation in the presence of TiO_2 thin films followed by further damage of the cell membranes (Xun *et al.*, 2008).

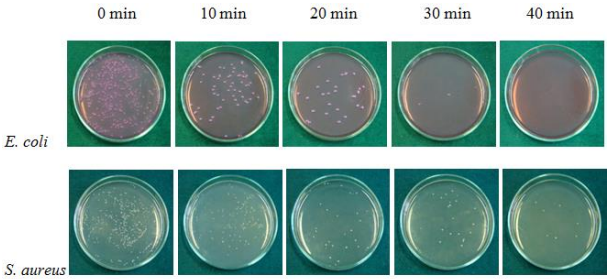

Figure 9. Growth of bacteria on agar plate observed after treatment with 40PVP/SnO_2/TiO_2 composite thin films against *E. coli* and *S. aureus* under UV irradiation.

4. Conclusions

The composite films of PVP-doped SnO_2/TiO_2 and undoped films coated on glass fibers were prepared by sol-gel and dip-coating methods. Films were heated at 600 °C for 2 h at a heating rate of 10 °C/min to form the anatase phase. The 40PVP/SnO_2/TiO_2 composite film had narrow band gap energy, high crystallinity of the anatase phase, and small crystallite size which may have contributed to the highest photocatalytic activity. The antibacterial activity of the 40PVP/SnO_2/TiO_2 thin film had greater bacteria inactivation under UV irradiation than the undoped TiO_2 films. This result correlated well with the photocatalytic reaction on MB degradation. The experimental results demonstrated that the synthesized structures exhibited antibacterial response against both gram positive and gram negative bacteria. It was found that the 40PVP/SnO_2/TiO_2 film had a higher antibacterial effect on gram negative than gram positive bacteria. The 40PVP/SnO_2/TiO_2 films coated on glass fibers are expected to be applied as an antibacterial photocatalyst for water purification.

Acknowledgements

The authors gratefully acknowledge support by the Department of Materials Engineering, Faculty of Engineering and Architecture, Rajamangala University of Technology Isan.

References

Chen, L. C., Tsai, F. R., Fang, S. H., & Ho, Y. C. (2009). Properties of sol–gel SnO_2/TiO_2 electrodes and their photoelectrocatalytic activities under UV and visible light illumination. *Electrochim Acta, 54*, 1304–1311.

Gao, P., Liu, J., Zhang, T., Sun, D. D., & Ng, W. (2012). Hierarchical TiO_2/CdS "spindle-like" composite with high photodegradation and antibacterial capability under visible light irradiation. *Journal of Hazardous Materials, 229–230*, 209–216.

Gentile, G. J., & Fidalgo, M. M. (2016). Enhanced retention of bacteria by TiO_2 nanoparticles in saturated porous media. *Journal of Contaminant Hydrology, 40*, 3274 – 3280.

Jaiswal, R., Patel, N., Kothari, D. C., & Miotello, A. (2012). Improved visible light photocatalytic activity of Ti O_2 co–doped with vanadium and nitrogen. *Applied Catalysis B: Environmental, 126*, 47-54.

Li, Q., Mahendra, S., Lyon, D. Y., Brunet, L., Liga, M. V., Li, D., & Alvarez, P. J. J. (2008). Antimicrobial nanomaterials for water disinfection and microbial control: Potential applications and implications. *Water Research, 42*, 4591–4602.

Liuxue, Z., Peng, L., & Zhixing, S. (2006). Photocatalysis anatase thin film coated PAN fibers prepared at low temperature. *Materials Chemistry and Physics*, *98*, 111-115.

Qin, H. L., Gu, G. B., & Liu, S. (2008). Preparation of nitrogen-doped titania with visible-light activity and its application. *Comptes Rendus Chimie, 11*, 95-100.

Ramani, M., Ponnusamy, S., & Muthamizhchelvan, C. (2012). From zinc oxide nanoparticles to microflowers: A study of growth kinetics and biocidal activity. *Materials Science and Engineering C, 32*, 2381–2389.

Rajakumara, G., Rahumana, A., Roopanb, S. M., Khannac, V. G., Elangoa, G., Kamaraja, C., . . . Velayuthama, K. (2012). Fungus-mediated biosynthesis and characterization of TiO_2 nanoparticles and their activity against pathogenic bacteria. *Spectrochimica Acta Part A, 91*, 23– 29.

Sikong, L., Masae, M., Kooptarnond, K., Taweepreda, W., & Saito, F. (2012). Improvement of hydrophilic property of rubber dipping former surface with Ni/B/TiO_2 nano-composite film. *Applied Surface Science, 258*, 4436–4443.

Vaiano, V., Sacco, O., Sannino, D., Navarra, W., Daniel, C., & Venditto, V. (2017). Influence of aggregate size on photoactivity of N-doped TiO_2 particles in aqueous suspensions under visible light irradiation. *Journal of Photochemistry and Photobiology A: Chemistry, 336*, 191–197.

Valentin, C. D., Finazzi, E., Pacchioni, G., Sellonib, A., Livraghi, S., M. Paganini, C., & Giamello, E. (2007). N-doped TiO_2: Theory and experiment. *Chemical Physics, 339*, 44–56.

Wang, H., Gao, X., Duan, G., Yang, X., & Liu, X. (2015). Facile preparation of anatase–brookite–rutile mixed-phase N-doped TiO_2 with high visible-light photocatalytic activity. *Journal of Environmental Chemical Engineering, 3*, 603-608.

Xin, B., Ding, D., Gao, Y., Jin, X., Fu, H., & Wang, P. (2009). Preparation of nanocrystalline Sn–TiO_{2-X} via a rapid and simple stannous chemical reducing route. *Applied Surface Science, 255*, 5896–5901.

Xun, W., & Wengi, G. (2008). Bactericidal and photocatalytic activity of Fe^{3+}-TiO_2 thin films prepared by the sol-gel method. *Journal of Wuhan University of Technology Materials Science Edition*, 155–158.

Ying, J., Bai, H., Jiang, Q., & Lian, J. (2008). Visible-light photocatalysis in nitrogen–carbon-doped TiO_2 films obtained by heating TiO_2 gel-film in an ionized N_2 gas. *Thin Solid Films, 516*, 1736–1742.

Zaleska, A. J., Sobezak, W., Grabowska, E., & Hupka, J. (2008). Preparation and photocatalytic activity of boron modified TiO_2 under UV and visible light. *Applied Catalysis B: Environmental, 78*, 92–100.

Zhang, W., Chen, Y., Yu, S., Chen, S., & Yin, Y. (2008). Preparation and antibacterial behavior of Fe^{3+}-doped nanostructured TiO_2 thin films. *Thin Solid Films, 516*, 4690–4694.

Zhang, X., & Liu, Q. (2008). Preparation and characterization of titania photocatalyst co-doped with boron, nickel, and cerium. *Materials Letter, 6*, 2589–2592.